AIAA SciTech Forum
23-27 January 2023, National Harbor, MD & Online
AIAA SCITECH 2023 Forum

10.2514/6.2023-1263

Combustion Chamber Fatigue Life Analysis for Reusable Liquid Rocket Engines (LREs)

Mateusz T. Gulczyński[1] and Jörg R. Riccius[2],
Günther Waxenegger-Wilfing[3], Jan C. Deeken[4], Michael Oschwald[5]
German Aerospace Research Center DLR Lampoldshausen, 74239 Hardthausen am Kocher, Germany

To increase liquid rocket engines (LREs) lifetime capability and allow for reusability applications, the efficient evaluation of the most critical subcomponents' remaining useful life plays a vital role. Regeneratively cooled combustion chamber (CC) wall must withstand extremely high loads emerging from a massive temperature gradient between the hot gas and the low temperature of the coolant. The combined loading and unloading operations, together with high temperature and rate dependent inelastic strain, significantly lessen the combustion chamber inner liner life. Within the presented research, the post-processing model was developed for low cycle fatigue (LCF) evaluation of the reusable LRE's combustion chamber walls. The proposed damage accumulation model is based on the amalgamation of Bonora-Gentile-Pirondi (2004) and Dufailly-Lemaitre (1995) methods, and it incorporates ductile and brittle damage components which are embedded in the post-processing method. Moreover, the required numerical calculation time is further decreased on account of the proposed routine which allows for analysis of only two initial numerically acquired FE cycles. The obtained results based on the developed method combined with coupled thermal-structural quasi 2D Finite Element Analysis (FEA) of the nozzle throat cross-section, were confirmed to be in good agreement with the validation data acquired from the M51 thermo-mechanical laboratory site at DLR Lampoldshausen. The proposed model can be successfully applied for a quick evaluation of the remaining useful life of the CC wall for various rocket engine architectures.

[1] Research Scientist, Institute of Space Propulsion, Rocket Propulsion Department
PhD Student at RWTH Aachen University, Faculty of Mechanical Engineering

[2] Structures Team Technical Leader, Rocket Propulsion Department

[3] Head of System Analysis and Control Research Group, Institute of Space Propulsion, Rocket Propulsion Department
Professor at the University of Würzburg, Institute of Computer Science, Digital methods in the modeling and control of space propulsion

[4] Acting Dept. Head Rocket Engine Systems, Institute of Space Propulsion
Professor at RWTH Aachen University, Faculty of Mechanical Engineering, Institute of Jet Propulsion and Turbomachinery

[5] Coordinator Rocket Propulsion, Institute of Space Propulsion, Rocket Propulsion Department
Professor at RWTH Aachen University, Faculty of Mechanical Engineering, Institute of Jet Propulsion and Turbomachinery

Nomenclature

α	=	damage evolution exponent
β	=	parameter calculated for temperature interpolation
γ and X_∞	=	kinematic hardening parameters
Δt	=	time increment
$\dot{\varepsilon}$	=	strain rate (can be also ^{e}lastic, ^{p}lastic, thermal)
ε_{th}	=	damage threshold strain
ε_D or ε_{th}	=	damage threshold strain
ε_r or ε_f	=	theoretical strain to failure that a ductile material would exhibit under uniaxial stress
$\dot{\varepsilon}_{ij}^{p}$	=	plastic strain rate second order tensor
K and N	=	viscosity parameters
ν	=	Poisson's ratio
σ_d or σ_{ij}^{D}	=	deviatoric stress – stress component which changes the shape of a given specimen
σ^{eff}	=	stress applied to undamaged material to strain occurrence in damaged material under the nominal stress
σ_{eq}	=	equivalent stress
σ_H	=	hydrostatic stress – stress component which changes the volume of the given specimen.
σ_{ij}^{D}	=	stress deviator
σ_{kk}	=	stress with two identical indices kk
σ_s	=	actual yield stress
σ_u	=	ultimate stress
D	=	decrease of the elastic modulus $\acute{E}$ induced by damage
D_0	=	initial damage
D_{cr}	=	critical damage
$\dot{D}$	=	damage rate, kinetic damage
D_{total}	=	total damage
E_0 or E	=	Young's modulus where D=0, undamaged material
E_{eff} or $\widetilde{E}$	=	Young's modulus of a damaged material
f	=	yield function
$J_{xTemp,K\Rightarrow xK}$	=	temperature field for temp. "x"
$\dot{p}$	=	accumulated plastic strain rate
Q	=	heat flux
R_ν or $f\left(\frac{\sigma_m}{\sigma_{eq}}\right)$		triaxiality function
R_∞ and R_0	=	isotropic hardening or softening parameters
S an s	=	material fitting parameter
t	=	time
T	=	temperature
Y	=	damage energy release rate

Acronyms/Abbreviations

APDL	ANSYS Parametric Design Language
CC	Combustion Chamber
CDM	Continuum Damage Mechanics
FEM	Finite Element Method (FEA – Finite Element Analysis)
HCF	High Cycle Fatigue
LCF	Low Cycle Fatigue
LCH4	Liquid Methane
LOx	Liquid Oxygen
LREs	Liquid Rocket Engines (RLREs – Reusable Liquid Rocket Engines)
Prometheus	Precursor Reusable Oxygen Methane cost Effective propulsion System
RLV	Reusable Launch Vehicle
Solid185	Eight nodes having three degrees of freedom at each node
TMF	Thermo-Mechanical Fatigue
VLCF	Very Low Cycle Fatigue

I. Introduction

The newly developed reusable liquid rocket engines (RLREs) necessitate the commencement of reliable methods to evaluate the critical sub-components' remaining useful life. For regeneratively cooled combustion chamber (CC), an exceptionally high load reduces considerably the life of the inner liner. The load is predominantly a resultant of the substantial temperature gradient between the hot gas and the low temperature of the coolant, along with repeated loading and unloading operations combined with effects such as a viscoplastic strain – crucial to consider for reusable liquid rocket engines (LREs) applications [1].

Within presented study we evaluate CC fatigue life for reusable engines, comparable to Prometheus (Precursor Reusable Oxygen METHane cost Effective propUlsion System) – main stage of the European Ariane 6 with hardware components validated at several facilities in Lampoldshausen, e.g. P5 test bench shown in Figure 1. Prometheus is a regeneratively cooled 1MN thrust class engine, fueled with cryogenic liquid Methane/Oxygen (LCH4/LOX), which offers a reusability capacity of up to five missions. The turbomachinery is based on a classic gas generator open cycle, which empowers a mono-shaft turbopump for both propellants. Within a nominal combustion chamber pressure of 12MPa, the peak heat load in the nozzle throat area is higher than 80MW/m^2 [2], [3]. This engenders a large radial temperature gradient in the combustion chamber wall, causing an immense heat flux and thermal stresses, emerging the failure in the inner liner (Figure 1 A-A c.s.- LCF crack microscopic view). The presented cross-section of the CC cooling channels with a microscopic view of a Thermo-Mechanical Fatigue (TMF) cut-out, was tested to failure at the DLR Lampoldshausen laboratory test bench M51 (Figure 2) for validation data. Supplementary specification of the M51 test bench can be found in [4], [5].

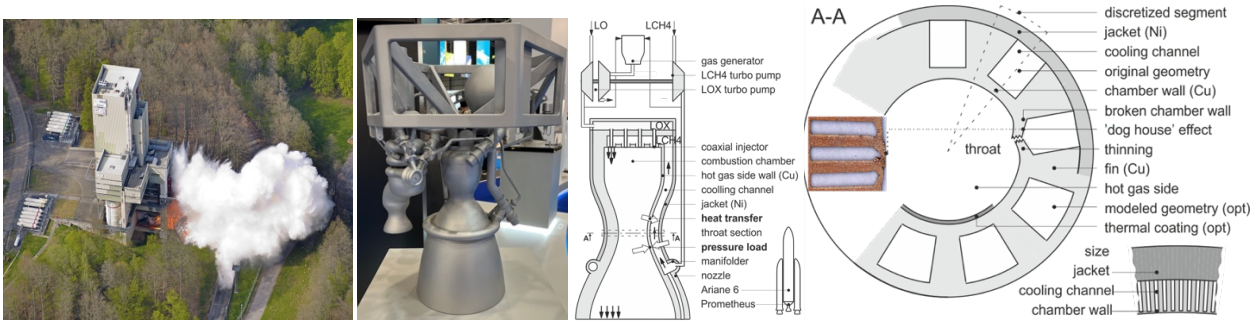

Figure 1 Left side: P5 testing facility at DLR Lampoldshausen for the first Prometheus engine test model (M1) Right side: Prometheus gas generator engine schematic with a regeneratively cooled combustion chamber cross-section (A-A) and a middle cross section of the TMF panel with visible "dog house" effect- LCF crack - microscopic view (left side of A-A) from DLR Lampoldshausen laboratory site M51 (M. T. Gulczyński et al.)

This paper is structured as follows:

- Section II. **Motivation and General Approach** – emphasizes main requirements imposed on the critical reusable LREs structures along with a general approach towards evaluation of the CC's fatigue life and RLRE's life cycle;

- Section III. **FE Plasticity Model and Discretization** – introduces a developed one way-coupled thermo-structural elastoplastic model, including: applied boundary conditions, laser loading sequence and a temperature profile;

- Section IV. **Fatigue Life Model** – highlights calculation methodology with applied constitutive model. LCF post-processing accumulative damage model conforms with Bonora-Gentile-Pirondi (2004), Dufailly-Lemaitre (1995);

- Section V. **Post-processing Analysis and Results**– encompasses applied methods with ductile and brittle damage components representation. Differentiation between two developed techniques is highlighted:
  - post-processing based on FE simulation with all cycles to failure;
  - post-processing based on two initial numerically acquired cycles- allowing faster fatigue life estimation;

- Section VI. **Conclusions** – features comparison of the post-processing and numerically obtained results along with laboratory tests of the CC type TMF panel (test bench DLR). The number of cycles to failure with a failure position for both: numerical method and laboratory tests is shown. Finally, the outlook for future studies is presented.

II. Motivation and General Approach

An increased operational and production costs associated with RLV technology development and flight qualification requirements motivate the research on more efficient numerical models to evaluate LRE's critical structures. To evaluate the remaining useful life of the RLRE's CC wall, a damage accumulation method is proposed with damage variables obtained by combining models in accordance with Bonora-Gentile-Pirondi (2004) for ductile failure and Dufailly-Lemaitre (1995) for brittle failure. The integration of a progressive accumulation of plastic strain in the course of cycling stress –is especially important for rocket engine components during their test phase, as well as to increase the reusability capacity of the future RLVs. The damage accumulation is determined by loading parameters: stress ratio, mean stress and loading sequence. In contrast to the originally proposed method, where damage parameter values are integrated as a state variable in the FEA, an alternative approach is presented, where damage parameter are integrated in the post processing stage to save numerical analysis time. The failure is related to total mechanical strain (ductile damage) and accumulated plastic strain (brittle damage + macro propagation part). To considerably reduce the analysis time, the calculation of the component's remaining useful life is further enhanced where only two initial numerically acquired cycles are integrated. The accumulated plastic strain approach (including both: the ductile and the brittle damage part) is applicable for LCF, but not for high cycle fatigue (HCF).

A time dependent model for RLV incorporates specific mission profiles: acceptance test (3-4 cycles 215- 890s), ascent phase (estimated 1 cycle, 100-130s) and retro propulsion manoeuvres (estimated 3 cycles, 30s). Accordingly, a reusable engine at 10 flight missions would have to withstand up to 43 cycles (Table 1) [6], [7].

Table 1 Product life cycle for reusable LRE (M. T. Gulczyński et al.)

	Product Life Cycle Event		Duration* s	No. of cycles*
Acceptance Test	Single MLC (Main Life Cycle) incl. hot fire test	Acceptance hot-fire test before the actual flight; Engine ground start hold-down with launch commit criteria abort; A single flight mission duration + several flight missions for reusable main stage engine;	215 →890	3→4
Ascent Phase	Lift-Off	Vertical take-off	0.2 →0.1	1
	Pitch Over	Constant pitch rate	11.8 →4.1	
	Pitch Constant	Transition to gravity turn	6 →3.3	
	Gravity turn	Angle of attack is zero	47 →42.5	
	Ascent	With stage separation	130 →100.2	
	Mission nominal time		165 →520	
Retro Propulsion Man.	Flip Over and Boost Back Burn Manoeuvre	Nitrogen thrusters used for flip over; ignition of 3 of 9 main engines (Falcon9 case); Re-ignition of three engines- ballistic re-entry	≅ 30	3
	Re-entry burn	Central engine is re-ignited shortly before landing		
	Touch down			

The components' degradation at each hot-fire test is activated by two fundamental failure mechanisms: cyclic strain-increase and time dependable strength-reduction. These are triggered by following principal failures: wear, erosion, creep, fatigue (with crack initiation and propagation) as well as a failure by thermal ageing [1], [6], [8], [9]. The most frequently encountered fatigue failures modes of RLRE's thrust chambers are:

(I) LCF resulting from a cyclic plastic deformation of the inner wall in the course of repeated operations;
(II) creep of the inner wall – resulting from high temperature rate dependent inelastic strain;
(III) thermal ratcheting – occurring due to a combination of cyclic thermal stress (secondary stress) superimposed on constant load-controlled stress (primary stress) [10].

A deformation increases progressively accumulating in the load-controlled stress direction applied as the number of cycles of the thermal stress grows [11]. This results in a cyclic accumulation of plastic strain in the inner wall. In the case of the double- wall thrust chamber (inner liner and outer jacket), the primary mode of failure is by bending, "dog house effect" (ratchetting and bulging into the hot gas) and rupture of the inner wall ligament [12].

III. Finite Element Plasticity Model and Discretization

With an increased number of cycles anticipated for reusable LRE, the coupling between plasticity models and damage is essential to forecast the nonlinear behavior of the CC liner material. The hereby presented model assumes a damage isotropy (microcracks and microviods are uniformly distributed in all directions), presupposed to be an adequate simplification for obtaining reliable results of the CC's critical number of cycles to failure. A continuum, plasticity-based model is applied to represent the elasto-plastic deformation of a CC. The high-conductivity copper-based alloy CuCrZr is used for the CC's inner liner, composed of chromium particles – preventing an extensive grain growth during the recrystallization process at increased temperature, as well as zirconium particles– which refine the grains and ties the oxygen within the structure. The foundation of the presented study is continuum plasticity model combined with finite element discretization, used to evaluate critical number of cycles to failure.

A. Continuum Plasticity Model

The elasto-plastic constitutive theory, incorporated in the model, focuses on evaluating the influence of irreversible damage corresponding to failure mechanisms that are observed in the CC structure under thermal and pressure loading conditions [13]. The deformation is defined with elastic, plastic and thermal components (strain rate decomposition):

$$\dot{\varepsilon} = \dot{\varepsilon}^{e} + \dot{\varepsilon}^{p} + \dot{\varepsilon}^{th} \tag{1}$$

These relate the objective stress rate to the elastic part of the deformation with a following equation:

$$\dot{\sigma} = C^{\sigma J} : (\dot{\varepsilon} - \dot{\varepsilon}^{p} - \dot{\varepsilon}^{th}) \tag{2}$$

A damage-caused reduction of the elastic stiffness is not considered in the Finite Element analyses. The yield surface evolution is controlled by the main hardening variable: plastic strain "ε^{pl}". Formulas applied for the FE analysis are presented in Table 2.

Table 2 Formulas incorporated into Finite Element analysis (M. T. Gulczyński et al.)

Nomenclature	Parameter	Calculation Formula	Unit	Eq. Nr.
Hydrostatic stresses	σ_H	$= \frac{\sigma_{11}+\sigma_{22}+\sigma_{33}}{3} = \frac{1}{3}tr(\sigma) = \frac{1}{3}I_1 = \frac{1}{3}\sigma_{kk}$	MPa	(3)
Von Mises equivalent stress	σ_{eq}	$= \sqrt{\frac{3}{2}\sigma_{ij}^{D}\sigma_{ij}^{D}}$	MPa	(4)
Stress deviator	σ_{ij}^{D}	$= \sigma_{ij} - \frac{1}{3}\sigma_{kk}\delta_{ij}$	MPa	(5)
Effective accumulated plastic strain rate ($\dot{p}_{(t)}$)	$\dot{p}$	$= \sqrt{\frac{2}{3}\dot{\varepsilon}_{ij}^{p}\dot{\varepsilon}_{ij}^{p}}\ ; \dot{p} = (\frac{f}{K})^{N}$		(6)
Strain hardening power law for 1-D case	ϵ_p	$= (\frac{\sigma-\sigma_y}{K})^{N}$ * "K" and "N" identified from tensile test curve	-	

B. Finite Element Discretization

The core section of the Thermo-Mechanical Fatigue panels, tested at DLR Lampoldshausen M51 laboratory site (Figure 2), is represented with CC's structural finite element model (FEM). The TMF panels constitute the cutout of the LRE- CC's inner liner with 5-7 cooling channels. To represent the hot gas medium, heat flux, as well as to simulate typical failure mechanisms such as a "dog-house" effect (visible on the right side of Figure 2), the cyclic laser heating on the surface is applied. The laboratory provides a reliable validation data which may be used for CFD, thermal and structural analysis, further successfully utilized as a substitution of the full-scale engine testing campaign [14].

Figure 2 Left side – Thermo-Mechanical Fatigue laboratory test set-up used for validation of the FE results. Middle – liquid booster nozzle throat TMF panel (CuCrZr): without coating (bottom), coated TMF panel (top). Right side – TMF cross section visible cooling channel deformation (M. T. Gulczyński et al.)

As highlighted in the center of Figure 2, the laser loaded surface of the liquid rocket nozzle throat TMF panel poses a cylindrical surface for tensile deformation accumulation in the middle part of the cooling channel. The core section of the TMF panel tested at DLR Lampoldshausen lab. – with structure type corresponding to Prometheus engine CC's cooling channels and the thin area – are represented with structural FEM model (as highlighted in Figure 3). The variables acquired during laboratory test runs of the TMF panel, and CuCrZr material are presented in Table 3 and Table 5. The viscosity parameters, along with hardening parameters, identified through the cyclic tension/compression test optimized by means of the least-square method, are incorporated in the theoretical model.

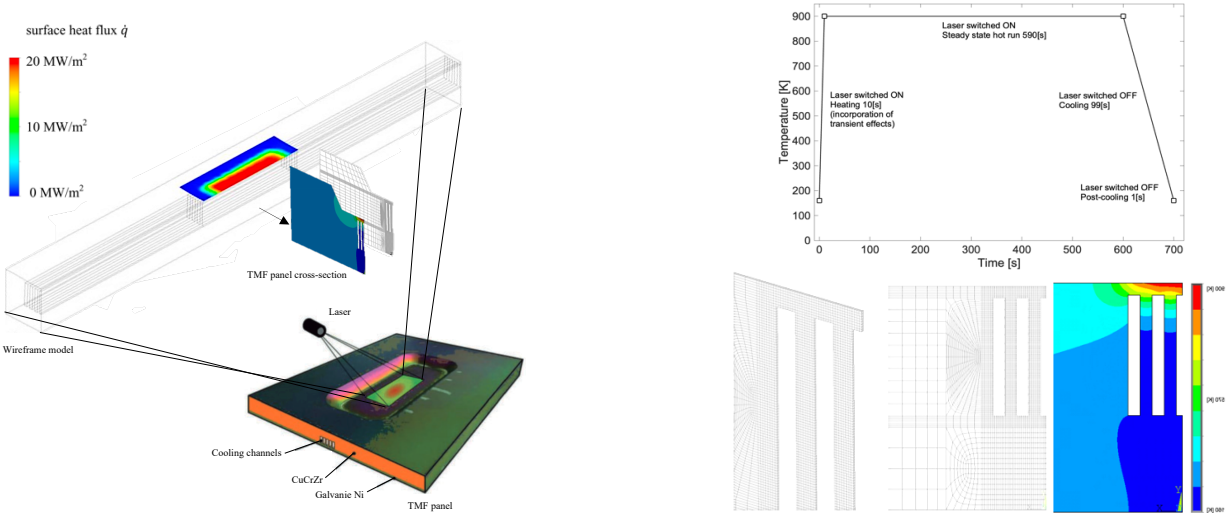

(a) **(b)**

Figure 3 (a) TMF schematic with wireframe model of nozzle throat section and heat flux boundary condition Q=20MW/m². Quasi-2-D FEM model cross-section with temperature distribution (partially adapted [15]) (b) Top – time dependency of the maximum TMF panel temperature, caused by laser loading for each fatigue-relevant cycle (Tmax=900K). Bottom – mesh of the quasi-2-D model (one element in the Z direction) 4782 8- node 3D elements. Temperature distribution for T_{max}= 900K, $T_{coolant}$= 160K. (M. T. Gulczyński et al.)

The model is meshed with 4782 "Solid185" elements (eight nodes having three degrees of freedom at each node). The boundary conditions are applied on the area on the face normal to the X direction, and the inlet surface is fixed in the transverse direction of the cooling channels. The coupling is implemented to allow for the same nodal temperature and pressure displacement in the X, Z nodal direction.

The material parameters (Table 3) were least-squares fitted from the results of uni-axial tests with the TMF panel material and used mainly for the FE analysis ("E" and "ν" also applied in the post processing). The numerically obtained results, applied to the post-processing analysis, include: time, stresses (incl. hydrostatic stress), elastic and plastic strains, Von Mises and equivalent plastic strains, plastic strain rate, local temperature.

Table 3 Structural material parameters least-squares-fitted from the isothermal fatigue (LCF) and tensile tests as used for the FE analysis (M. T. Gulczyński et al.)

Nomenclature	**Parameter**	**Unit**	**T= 300K**	**T= 700K**	**T= 900K**
Young's modulus	E	MPa	115680	113750	95100
Poisson's ratio	ν	-	0.3	0.3	0.3
Viscosity	K	MPa	570	3050	365
parameters	N	-	5.5	1.8	4.5
Yield stress	σ_s (or σ_y)	MPa	160.5	142.9	31.8
	R_∞	MPa	55	-10	-18
	R_0	MPa	-0.1	-5.0	-3.0
Kinematic hardening	X_∞	MPa	60.3	64.2	19.2
parameters	γ	-	300	700.8	620.6

IV. Fatigue Life Model

The proposed fatigue life accumulative damage model for LCF evaluation combines methods in accordance with Bonora-Gentile-Pirondi (2004) and Dufailly-Lemaitre (1995). The calculated variables are applied over numerous load cycles to project the probability of the crack initiation as well as to allow faster fatigue life evaluation of the CC component. Furthermore, the presented methodology is further developed to empower even faster estimation of the remaining useful life of the CC by data extrapolation (explained thoroughly in section V).

A. Damage potential

The evolution of damage is highly dependable on the selected damage potential. It is directly influenced by the damage "response" – resulting in damage increase progressing faster or slower with respect to deformation [16]. Thus, an accurate input data obtained from laboratory tests are pivotal in studies on damage evolution – foremost for ductile materials. The damage "D" is associated with a decrease of the elasticity modulus "$\acute{E}$" induced by the damage:

$$D = 1 - \frac{A_{\mathrm{eff}}}{A_0} = 1 - \frac{E_{\mathrm{eff}}}{E_0} \tag{7}$$

where "E_0" and "E_{eff}" are the Young's modulus of the undamaged and damaged materials respectively and "D" is damage variable [17]. The decrease of the effective Young´s modulus, resulting from the softening process induced by the damage "D", can be measured with uniaxial tests, assuming for damage variable a ratio of the damaged reference volume area "$A_D=1-A_{eff}$" to the nominal one. The variable "A_D" accounts for voids and microcracks which reduce the reference volume element (RVE) effective net resisting area and their mutual interactions. The damage variable is expressed as the material stiffness reduction. The stress-based definition of damage has a following form:

$$D = 1 - \frac{\sigma_s}{\sigma_u} \tag{8}$$

where "σ_s"– actual yield stress, "σ_u"– ultimate stress.
The theoretical value of the critical damage "D_{cr}=1" is smaller for most of the materials due to void and crack interactions [18]. Correspondingly, a critical damage for evaluated CC's wall CuCrZr material is equal to "D_{cr}=0.61".

B. Ductile Damage model based on Bonora (2004)

In accordance with Bonora, the damage rate can be calculated as:

$$\dot{D} = \alpha \left[\frac{D_{\mathrm{cr}} - D_0}{\ln\left(\varepsilon_{\mathrm{f}}/\varepsilon_{\mathrm{th}}\right)}\right] f\left(\frac{\sigma_{\mathrm{m}}}{\sigma_{\mathrm{eq}}}\right) \left(D_{\mathrm{cr}} - D\right)^{(\alpha-1)/\alpha} \frac{\dot{p}}{p} \tag{9}$$

Assuming a proportional loading "$f\left(\sigma_{\mathrm{m}}/\sigma_{\mathrm{eq}}\right) =$ constant", the equation can be written in the following form:

$$D = D_0 + (D_{cr} - D_0)\left\{1 - \left[1 - \frac{\ln\left(p/p_{th}\right)}{\ln\left(\varepsilon_f/\varepsilon_{\mathrm{th}}\right)} f\left(\frac{\sigma_{\mathrm{m}}}{\sigma_{eq}}\right)\right]^{\alpha}\right\} \tag{10}$$

By incorporating a uniaxial loading condition "$\mathrm{TF} = 0.333$" and "$f\left(\sigma_{\mathrm{m}}/\sigma_{\mathrm{eq}}\right) = 1.0$", it may be finally described as:

$$D = D_0 + (D_{cr} - D_0)\left\{1 - \left[1 - \frac{\ln\left(\varepsilon/\varepsilon_{\mathrm{th}}\right)}{\ln\left(\varepsilon_{\mathrm{f}}/\varepsilon_{\mathrm{th}}\right)}\right]^{\alpha}\right\}) \tag{11}$$

The damage variable Eq. (7) constitutes a definition for the damage, as it is possible to monitor the variation of the initial stiffness during strain accumulation in a tensile test executing partial unloading at given strain levels [17]. All required parameters: damage threshold strain "ε_{th}", uniaxial strain to failure "ε_f", critical damage "D_{cr}", damage evolution exponent "α", initial damage "D_0" (assumed to be 0 for a virgin material) must be identified in advance [17]. The example of damage evolution in function of strain for a given damage parameter set and a damage parameter exponent, is shown in Figure 4. The more detailed description of the damage evolution exponent influence in the frame of the presented research, is explained in the following section V and VI.

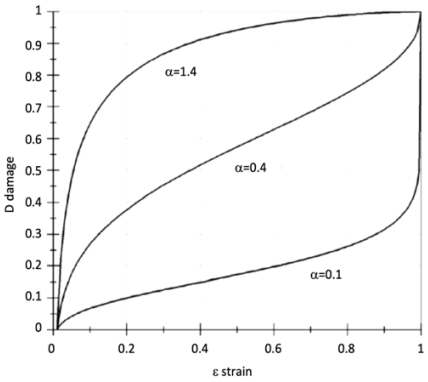

Figure 4 Example of different damage evolutions vs strain for a given damage parameter set (ε_{th} =0.01, ε_f =1.0, D_{cr} =1.0) and different choices of the α exponent (adapted from [19]) (M. T. Gulczyński et al.)

C. Brittle fatigue damage model based on Lemaitre-Desmorat and Dufailly-Lemaitre (1995)

In accordance with Dufailly and Lemaitre, the evolution of damage may be calculated as:

$$\dot{D} = \left(\frac{\sigma_{eq}^2 R_v}{2ES(1-D)^2}\right)^s \dot{p} \tag{12}$$

where "R_v" – triaxiality function, denotes as follows:

$$R_v = f\left(\frac{\sigma_\mathrm{m}}{\sigma_\mathrm{eq}}\right) = \frac{2}{3}(1+\nu) + 3(1-2\nu)\left(\frac{\sigma_\mathrm{m}}{\sigma_\mathrm{eq}}\right)^2 \tag{13}$$

For "$D<1$", Eq. (12) may be integrated to determine the condition of the crack initiation at a Very Low Cycle Fatigue (VLCF) process, when "σ_{eq}", "σ_H", "σ_m " and "p" are known [20]. The crack initiation is established by applying differential constitutive equations in a post processing step. The acquired data of the accumulated plastic strain rate "$\dot{p}_{(t)}$", the equivalent stress "σ_{eq}" and the hydrostatic stress "σ_H" must be extracted from the results of the Finite Element analysis. Moreover, the material parameters at a given temperature must be experimentally identified, that includes: "σ_s" (plastic threshold), "E", "S", "s" (exponent determined from fracture conditions). The parameters are to be determined from a strain-controlled tension-compression test, at constant amplitude of strain.

The complete set of equations for estimating the critical number of cycles to failure of the CC's inner liner are presented in Table 4.

Table 4 Equations for damage and critical fatigue life evaluation (M. T. Gulczyński et al.)

Nomenclature	**Parameter**	**Calculation Formula**	**Eq. Nr.**
Decrease of elastic modulus $\tilde{E}$ induced by damage (IAW Lemaitre)	D	$= 1 - \frac{\tilde{E}}{E}$	
	D_c	$= 1 - \frac{\sigma_{r(upture\ engineering\ stress)}}{\sigma_{u(niaxial\ max\ stress)}}$	(14)
Damage evolution for the uniaxial loading case R_v=1;(IAW Bonora)	D_{du}	$= D_{cr}\{1 - [1 - \frac{\ln\left(\frac{\varepsilon}{\varepsilon_{th}}\right)}{\ln\left(\frac{\varepsilon_f}{\varepsilon_{th}}\right)}]^\alpha\}$	(15)
Triaxiality function	R_v	$= \frac{2}{3}(1+\nu) + 3(1-2\nu)(\frac{\sigma_H}{\sigma_{eq}})^2$	(16)
Kinetic damage or periodic loading (IAW Lemaitre)	$\dot{D}$	$= \left(\frac{\sigma_{eq}^2 R_v}{2ES(1-D)^2}\right)^s \dot{p}$	(17)
Kinetic damage evolution law (IAW Bonora)	$\dot{D}$	$= \alpha \frac{(D_{cr}-D_0)^{\frac{1}{\alpha}}}{\ln\left(\frac{\varepsilon_f}{\varepsilon_{th}}\right)} R_v (D_{cr}-D)^{\frac{\alpha-1}{\alpha}} \frac{\dot{p}}{p}$	(18)

V. Post-processing Analysis and Results

As highlighted in the flow-chart Figure 5, the methodology to calculate the critical number of cycles to failure was divided into two methods: post-processing with all FE cycles incorporated in calculating a damage potential and critical fatigue life; post-processing studies where only two initial numerically acquired cycles are comprised, allowing for a quick estimate of the critical fatigue life based on the damage potential. Both methods were compered and validated with TMF Panel M51 laboratory results.

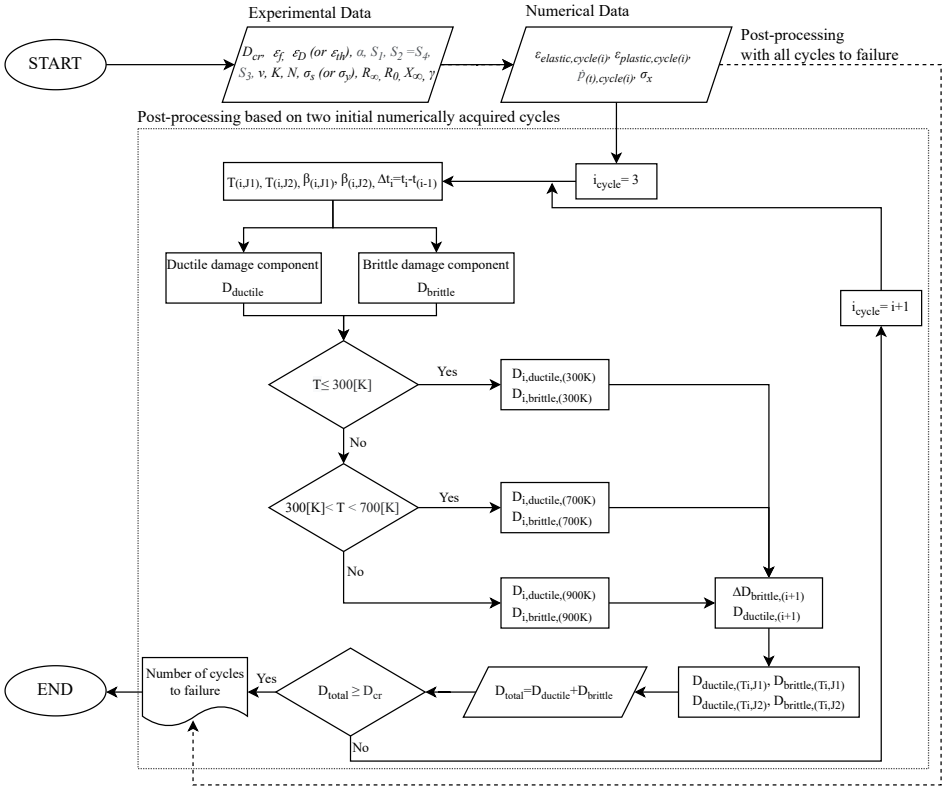

Figure 5 Flow-chart – post-processing developed method to evaluate critical damage and number of cycles to failure based on two initial numerically acuiqred cycles (M. T. Gulczyński et al.)

The generalized damage evolution model is formalized as follows:

$$D_{total} = D_{ductile} + D_{brittle} \tag{19}$$

where "D_{total}" denotes the total amount of brittle and ductile damage (equation expressed in its incremental form). The basic material parameters: "σ_s", "E", "S", "s", as highlighted in Table 5, are experimentally acquired from uniaxial tension-compression LCF tests, as in [21]. These are subsequently integrated into damage evolution equations in the post-processing CC's fatigue life evaluation, to allow an assessment of the crack initiation and propagation.

Table 5 Structural material parameters least-squares fitted from uniaxial fatigue & tensile tests (Gulczyński)

Nomenclature	Parameter	Unit	T= 300K	T= 700K	T= 900K
Critical damage value at tensile test	D_{cr}	-	0.50	0.38	0.61
Theoretical strain to failure that a ductile material would exhibit under uniaxial stress	ε_f	-	0.24	0.24	0.16
Damage threshold strain	ε_D (or ε_{th})	-	0.002	0.002	0.0008
Damage exponent	α	-	0.4	0.46	0.14
Material fitting parameter	S_1 (or "S")	MPa	49	17	3
	$S_2 = S_4$ (or "s")	-	1	1	1
	S_3 (or "S")	MPa	8	0.8	0.36

A. Ductile damage component "$D_{ductile}$"

The ductile damage is calculated in accordance with damage evolution model introduced by Bonora-Gentile-Pirondi (2004) for a uniaxial loading case. The largest deformation in the CC is anticipated for the circumferential (hoop) direction – equivalent to lateral direction of the TMF panel, with strain *"ε_x"* analysed in the x- direction.

$$D_{ductile,(i+1)} = D_0 + (D_{cr} - D_0)\left\{1 - \left[1 - \frac{\ln(\varepsilon(i+1)/\varepsilon_{\mathrm{th}})}{\ln(\varepsilon_{\mathrm{f}}/\varepsilon_{\mathrm{th}})}\right]^{\alpha}\right\} \tag{20}$$

Considering that "D_0=0" for the virgin material, the equation may be written as:

$$D_{ductile,(i+1)} = D_{cr}\left\{1 - \left[1 - \frac{\ln(\varepsilon_{(i+1)}/\varepsilon_{\mathrm{th}})}{\ln(\varepsilon_{\mathrm{f}}/\varepsilon_{\mathrm{th}})}\right]^{\alpha}\right\} \tag{21}$$

Within uni-axial material tests of the CC's copper-based alloy CuCrZr, three primary temperatures are recognized and further applied to the post-processing fatigue life analysis: T1 = 300K, T2= 700K, T3 = 900K. Subsequently, the following temperature fields are defined: "$J_{300K\Rightarrow700K}$" for the temperature between 300K and 700K; "$J_{700K\Rightarrow900K}$" for the temperature between 700K and 900K. An integration of temperature fields as well as material parameters "$\varepsilon_{\mathrm{th}}$" and "$\varepsilon_{\mathrm{f}}$" (constant at designated temperature state) along with strains "ε" extracted from FE analysis, provides a following formulation:

$$\begin{cases} D_{i,ductile,(300K)} = D_{cr}\left\{1 - \left[1 - \frac{\ln(\varepsilon_{(i+1)}/\varepsilon_{th})}{\ln(\varepsilon_f/\varepsilon_{th})}\right]^{\alpha}\right\} \\ \qquad\qquad \downarrow J_{300K\Rightarrow700K} \\ D_{i,ductile,(700K)} = D_{cr}\left\{1 - \left[1 - \frac{\ln(\varepsilon_{(i+1)}/\varepsilon_{th})}{\ln(\varepsilon_f/\varepsilon_{th})}\right]^{\alpha}\right\} \\ \qquad\qquad \downarrow J_{700K\Rightarrow900K} \\ D_{i,ductile,(900K)} = D_{cr}\left\{1 - \left[1 - \frac{\ln(\varepsilon_{(i+1)}/\varepsilon_{th})}{\ln(\varepsilon_f/\varepsilon_{th})}\right]^{\alpha}\right\} \end{cases} \tag{22}$$

Determined by temperature field "$J_{300K\Rightarrow700K}$" or "$J_{700K\Rightarrow900K}$" and defined temperature "T_i" (T_i is equal to T_1= 300K or T_2=700K or T_3=900K), the following parameters are calculated:

$$\begin{cases} T_{i,J1} = \beta * T_1 + (1-\beta) * T_2 \\ T_{i,J2} = \beta * T_2 + (1-\beta) * T_3 \end{cases} \tag{23}$$

which can be written as:

$$\begin{cases} \beta_{i,J1} = \frac{T_{i,J1} - T_2}{T_1 - T_2} \\ \beta_{i,J2} = \frac{T_{i,J1} - T_3}{T_2 - T_3} \end{cases} \tag{24}$$

By embodying parameter "β", a ductile damage is finally determined with the following linear interpolation equations:

$$\begin{cases} D_{ductile,(Ti,J1)} = \beta_{i,J1} * D_{i,ductile\,(300K)} + (1-\beta_{i,J1}) * D_{i,ductile\,(700K)} \\ D_{ductile,(Ti,J2)} = \beta_{i,J2} * D_{i,ductile\,(700K)} + (1-\beta_{i,J2}) * D_{i,ductile\,(900K)} \end{cases} \tag{25}$$

B. Brittle damage component "$D_{brittle}$"

Zero brittle damage is assumed for the virgin state of the material "$D_{brittle,0}=0$". The subsequent values of the brittle fatigue damage are determined incrementally:

$$D_{brittle,(i+1)} = D_{brittle,i} + \Delta D_{brittle,(i+1)} \tag{26}$$

where, "$D_{brittle,i}$" is the value of brittle damage at the i-th converged substep of the FE analysis, and the damage increment "$\Delta D_{brittle,(i+1)}$" is calculated based on the damage rate evolution equation of Dufailly-Lemaitre (1995):

$$\Delta D_{brittle,(i+1)} = \dot{D}_i \Delta t_i = (\frac{Y_{(i+1)}}{S})^s \, \dot{p}_{(t)} \, \Delta t_i \tag{27}$$

In dependency on a given material temperature condition (as highlighted in Table 5 for temperature condition of e.g. 900K "$S=S_1=3$", "$S=S_2=1$"), the damage exponent material fitting parameters "S" and "s" are employed. The accumulated plastic strain rate "$\dot{p}_{(t)}$" is extracted from the FE analysis at a given condition. In the aftermath, the strain energy density release rate "Y" is defined:

$$\mathrm{Y} = \frac{\sigma_{eq}^2 R_v}{2E(1-D)^2} \tag{28}$$

The incremental brittle damage equation is calculated with:

$$\Delta D_{brittle,(i+1)} = \left(\frac{\sigma_{eq,i}^2 R_{v,i}}{2ES}\right)^s \, \dot{p}_{(t)} \, \Delta t_i \tag{29}$$

where "R_v" is the triaxiality function:

$$R_v = \frac{2}{3}(1+\nu) + 3(1-2\nu)(\frac{\sigma_H}{\sigma_{eq}})^2 \tag{30}$$

and "Δt_i" represents the time increment written as:

$$\Delta t_i = t_i - t_{i-1} \tag{31}$$

In contrast to the original equation Eq. (17) by Dufailly-Lemaitre for damage rate calculation, where a value of "$(1\text{-}D)^2$" is applied as a conversion factor between the effective and a classical stress, in equation Eq. (29) the conversion factor is omitted, as a classical stress values are extracted from the FE analysis.
Finally, a linear interpolation is used to account for the temperature dependency of the brittle damage expressed as:

$$\begin{cases} D_{brittle,(Ti,J1)} = \beta_{i,J1} * D_{i,brittle\,(300K)} + (1-\beta_{i,J1}) * D_{i,brittle\,(700K)} \\ D_{brittle\,,(Ti,J2)} = \beta_{i,J2} * D_{i,brittle\,(700K)} + (1-\beta_{i,J2}) * D_{i,brittle\,(900K)} \end{cases} \tag{32}$$

C. Post-processing results

Owing to substantial computational cost inherent in FE calculation of the material's slow progressive damage over a large number of load cycles, an improved method is proposed encompassing a small part of the numerically calculated loading history. Within the newly proposed method, two initial numerically acquired cycles are incorporated into the post processing damage-parameter fatigue life analysis. The total damage value for cycle number 3 and its follow-on cycles is calculated by assuming the same stress-strain behaviour of the hysteresis loop as in the 2nd cycle until the critical damage is reached (D_{cr}=0.61). The variables "$\varepsilon_{elastic,cycle(i)}$", "$\varepsilon_{plastic,cycle(i)}$" and "$\dot{p}_{(t),cycle(i)}$" are updated in accordance with Eq. (33), and the remaining numerical parameters are reused from cycle number 2 for each sub-step of cycle number 3 and higher.

$$\begin{cases} \varepsilon_{elastic,cycle(i)} = \left(\varepsilon_{elastic,cycle(i-1)} - \varepsilon_{elastic,cycle(i-2)}\right) + \varepsilon_{elastic,cycle(i-1)} \\ \varepsilon_{plastic,cycle(i)} = \left(\varepsilon_{plastic,cycle(i-1)} - \varepsilon_{plastic,cycle(i-2)}\right) + \varepsilon_{plastic,cycle(i-1)} \\ \dot{p}_{(t),cycle(i)} = \left(\dot{p}_{(t),cycle(i-1)} - \dot{p}_{(t),cycle(i-2)}\right) + \dot{p}_{(t),cycle(i-1)} \end{cases} \quad (33)$$

The validation of the proposed method is conducted by the post-processing damage evolution model with all numerically acquired cycles and subsequently – with laboratory outcome. The results of both methods with damage evolution in function of critical cycles number for four nodes in circumferential direction, are presented in diagram Figure 6 (combined damages). The stress-strain curves along with a total damage propagation (sum of ductile and brittle damage) in dependency on the accumulated plastic strain for critical damage Dcr=0.61, are presented in Appendix – Figure 8 and Figure 9.

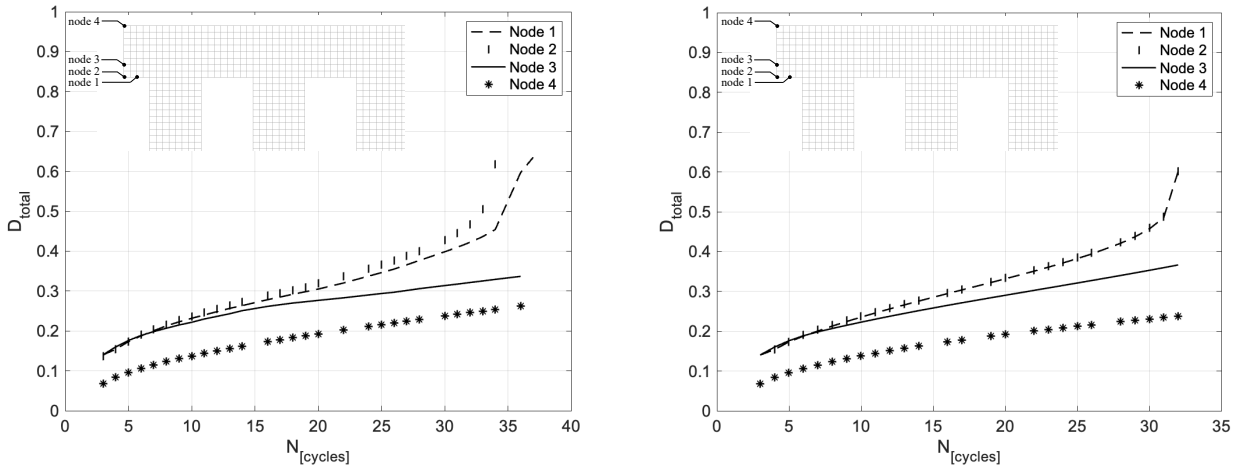

Figure 6 Combined results for nodes 1, 2, 3, 4 with number of cycles until critical damage occurs, based on (a) all numerically acquired cycles and (b) based on two-numerically acquired cycles(M. T. Gulczyński et al.)

The critical point of the CC with a lowest fatigue life, was identified at "node 2" (Figure 6). Two additional points, in the thickness direction of the wall – up to node 4, situated at the TMF panel's laser loaded side, were further assessed. Similarly to previously presented studies [22], within proposed model it was found that the ductile damage evolution constitutes a dominant failure, whereas a brittle part of the damage is found to be insignificant. On the laser loaded side – node 4 – with smaller damage evolution exponent "$\alpha \approx 0.14$" (damage evolution values in Table 5), a low initial damage rate is obtained which quickly expands as the failure strain is reached (not visible on the graph). The initial slow and localized nucleation phase is followed by either a rapid void coalescence or inter-void ligament fracture. At node 1 and node 2 – inside the cooling channels area, where the damage evolution exponent is higher "$\alpha \approx 0.4$", the extensive void nucleation stage and coalescence occurs as a consequence of the necking of the inter-void ligament [23]. As highlighted in Appendix, the brittle failure is smaller at node 2 when compared to damage evolution on the laser loaded side – that is node 4. Similarly with laboratory results, the failure location for both post-processing methods is in the middle cooling channel with critical number cycles of 34 and 32 respectively (Figure 6).

VI. Conclusions

The research effort demonstrated a newly developed post-processing method capable of a quick estimation of a remaining useful life in the LRE's component subjected to high thermo-mechanical loads. The post-processing method with calculations based on initial two numerically obtained cycles shows a good agreement with a post-processing model where all numerically acquired cycles are incorporated – 32 cycles until failure predicted for former versus 34 cycles until failure obtained for latter. Consequently, newly developed coupled thermo-structural quasi 2D FE model, with a fatigue life prediction model based on damage mechanics, allows to efficiently simulate a damage propagation of a RLRE's combustion chamber with an exact failure location.

The proposed model comprising a full loading cycle with pre-cooling, start-up, hot run (due to laser loading of the TMF panel) and post-cooling, was validated with TMF panels tested at DLR Lampoldshausen, where a critical failure in the combustion chamber inner wall was recorded at 87 cycles for the fatigue-relevant temperature of 900K, whereas circa 34 cycles until crack initiation was obtained for post-processing methods. In Figure 7, the combined results of laboratory tests and post-processing method was presented. Due to large temperature driven cyclic loading, a significant deformation leading to low cycle fatigue failure is recorded in the CC middle section thin wall area.

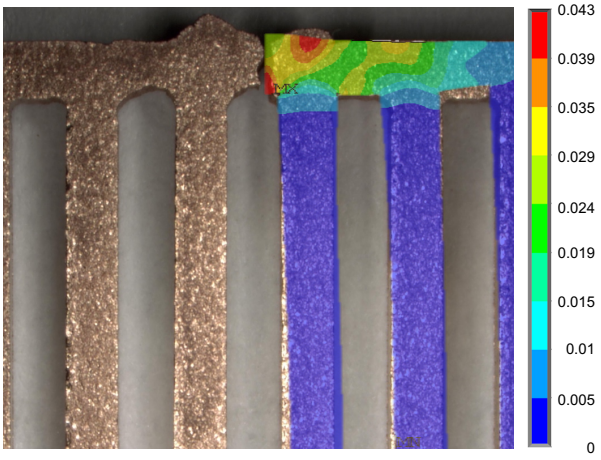

Figure 7 CC type panel cross section with cooling channels visible deformation (M51 DLR Lampoldshausen) combined with post-processing numerical results total mechanical strain at 34 cycles (M. T. Gulczyński et al.)

As may be observed in the Appendix – hysteresis loops, the unsymmetric cycles of stress between the limits causes progressive stable ratchetting in the mean stress direction (e.g. Figure 9b and c). Furthermore, for nodes 2 and 3, a plastic shakedown behaviour can be observed along with a predominant ratcheting response (Figure 9). Presumably, the annealed metal tends to soften in direction of the stable limit under plastic strain-controlled loading. By comparing Figure 8 and Figure 9 it may be noticed, that the prediction of the critical damage and number of cycles to failure is less accurate where the plastic shakedown with a small "$\Delta\varepsilon$" is observed. The stress-strain curve anisotropy in tension and compression tests is well-known source of ratcheting of structures [24]. The final deformation phase preceding the failure is often under large influence by the void coalescence process that rapidly pushed the net resisting area to instability. When a damage variable is approaching the critical value D_{cr}, the mutual interactions between microvoids engage to lessen the effective resisting section [18]. The presents of cycling stress (with tensile mean stress) combined with a ratcheting strain accumulation in the tensile direction as well as thinning of the components cross-section area, may lead to a permanent failure of the CC inner wall – as highlighted in Figure 7 [25].

Outlook

The long-term objective of the presented research encompasses further enhancement of damage simulation models with improved interplay between significant factors of elevated temperature, cyclic conditions and fatigue life mechanisms. In addition, an application of the model to other LRE's critical structures like turbopumps is envisaged (foreseen implementation to [26], [27], [28]) . Moreover, the future studies will include the evaluation of the given engine architecture supported by a system level simulation (SLS) and implementation of propulsion modeling tools, such as EcosimPro ESPSS - European Space Propulsion Simulation Toolkit. The extended research will enable faster and more accurate prediction of the LREs components remaining useful life for a given engine configuration.

Appendix

A. Stress-strain & Total damage–accumulated plastic strain diagrams based on all numerically acquired cycles

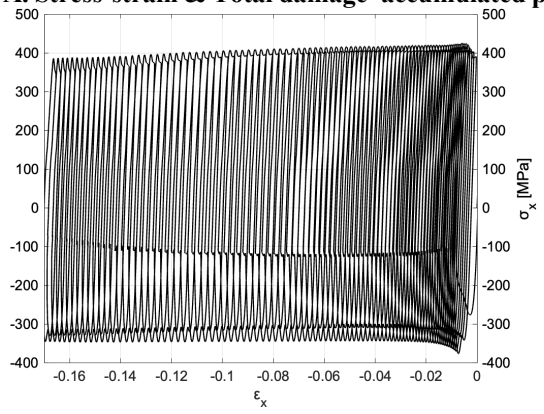

(a) Stress-strain at node 4

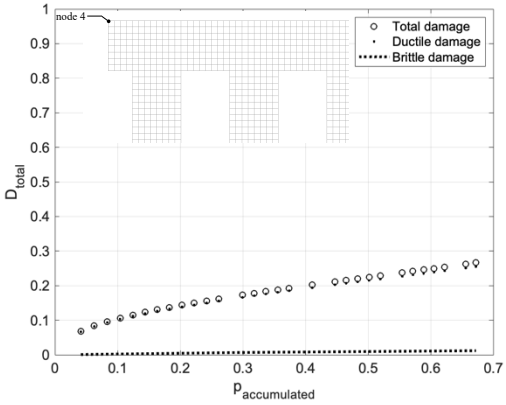

Damage in dependency on the accumulated plastic strain at node 4

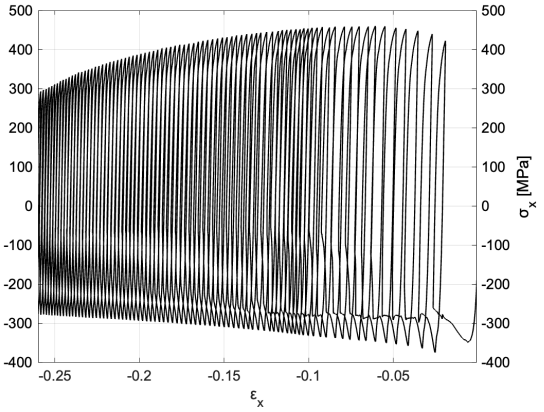

(b) Stress-strain at node 3

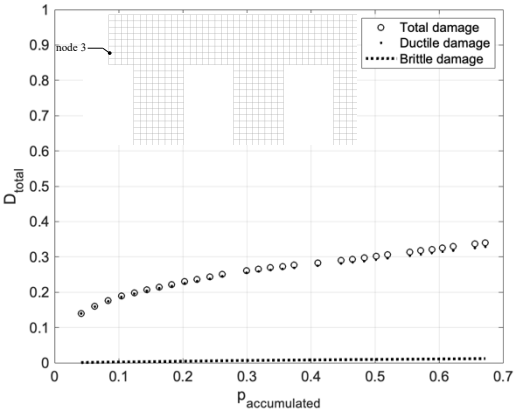

Damage in dependency on the accumulated plastic strain at node 3

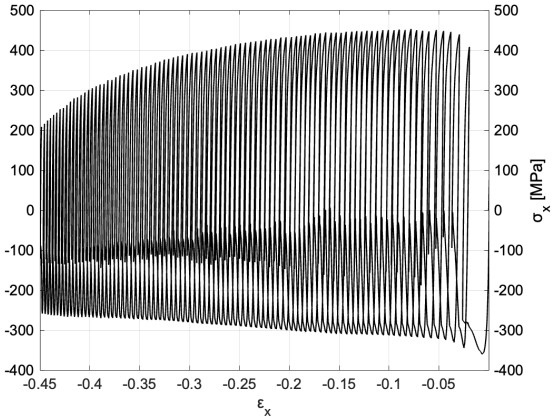

(c) Stress-strain at node 2

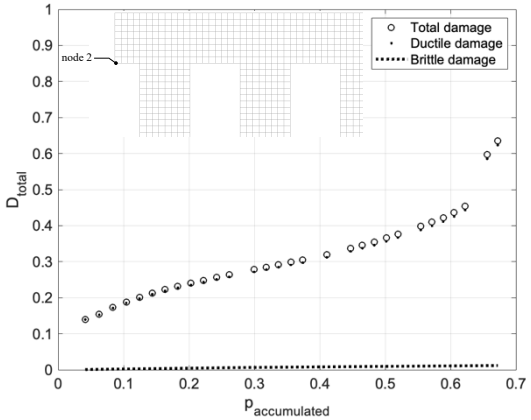

Damage in dependency on the accumulated plastic strain at node 2

Figure 8 Stress-strain in circumferential direction plotted based on all numerically acquired cycles to critical damage D_{cr}=0.61, along with total damage propagation (sum of ductile and brittle damage) in dependency on the accumulated plastic strain at (a) node 4, (b) node 3, (c) node 2 (failure point) (M. T. Gulczyński et al.)

B. Stress-strain & Total damage–accumulated plastic strain diagrams derived from two numerical cycles

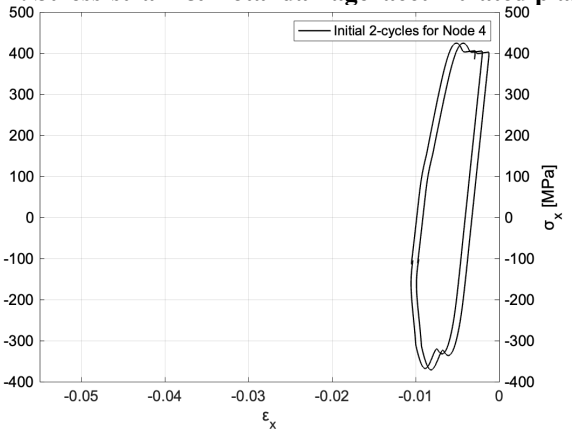

(a) Stress-strain at node 4 for cycles number 1 and 2

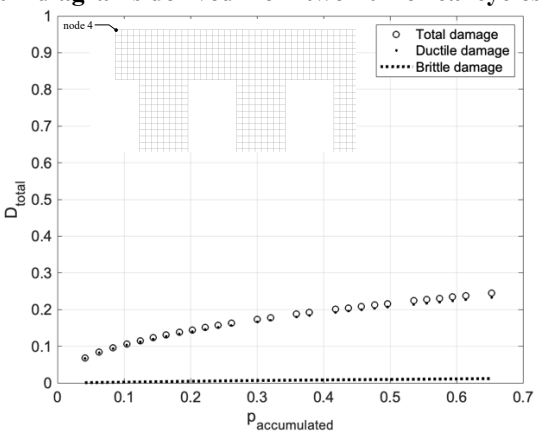

Damage in dependency on the accumulated plastic strain at node 4 based on two FE analysis cycles

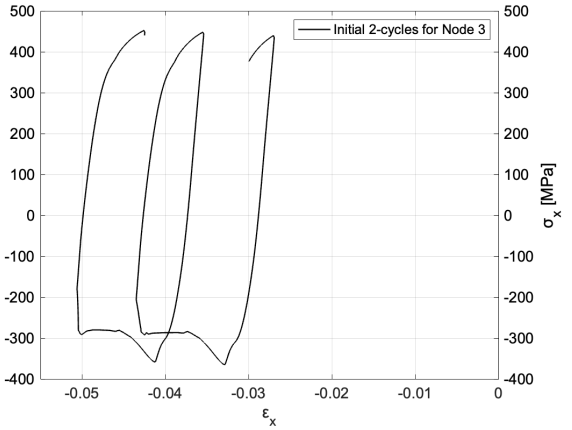

(b) Stress-strain at node 3 for cycles number 1 and 2

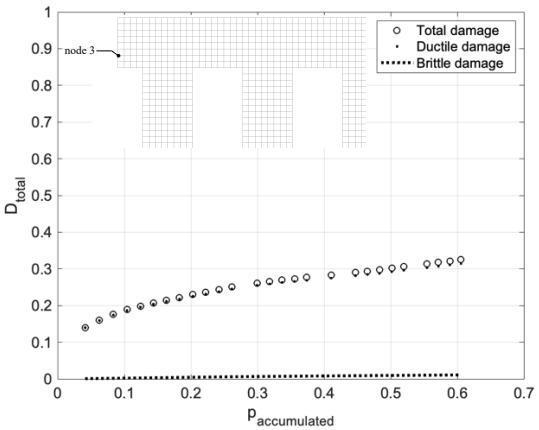

Damage in dependency on the accumulated plastic strain at node 3 based on two FE analysis cycles

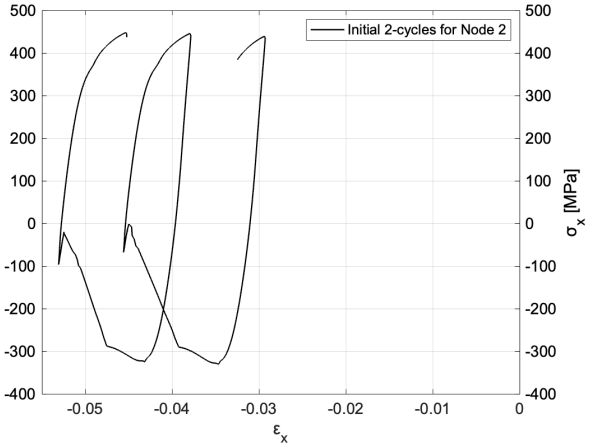

(c) Stress-strain at node 2 for cycles number 1 and 2

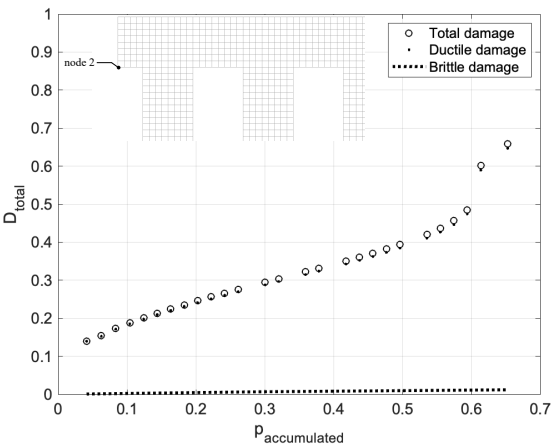

Damage in dependency on the accumulated plastic strain at node 2 based on two FE analysis cycles

Figure 9 Stress-strain curves in circumferential direction plotted based on two numerically acquired cycles, along with a total damage propagation (ductile and brittle damage)- accumulated plastic strain at (a) node 4, (b) node 3, (c) node 2 (failure point). (M. T. Gulczyński et al.)

Acknowledgments

The project leading to this paper has received funding from the European Union's Horizon 2020 research and innovation programme under the Marie Skłodowska-Curie grant agreement No 860956.

References

[1] M. T. Gulczynski *et al.*, "RLV applications: challenges and benefits of novel technologies for sustainable main stages," Oct. 2021. [Online]. Available: https://elib.dlr.de/148758/

[2] S. Callsen, S. Stappert, and M. Sippel, "Study on future European winged reusable launchers," pp. 1–14, 2022.

[3] A. Iannetti, N. Girard, C. Bonhomme, N. Ravier, E. Edeline, and F. De Vernon, "PROMETHEUS, A LOX/LCH4 REUSABLE ROCKET ENGINE," *7th Eur. Conf. Aeronaut. Sp. Sci.*, no. EUCASS 2017-537, pp. 1–9, 2017, doi: 10.13009/EUCASS2017-537.

[4] J. R. Riccius, E. B. Zametaev, W. Bouajila, and Q. Wargnier, "Inner liner temperature variation caused deformation localization effects in a multichannel model of a generic LRE wall structure," *50th AIAA/ASME/SAE/ASEE Jt. Propuls. Conf. 2014*, pp. 1–12, 2014, doi: 10.2514/6.2014-3988.

[5] R. G. Thiede, J. R. Riccius, and S. Reese, "Life prediction of rocket combustion-chamber-type thermomechanical fatigue panels," *J. Propuls. Power*, vol. 33, no. 6, pp. 1529–1542, 2017, doi: 10.2514/1.B36361.

[6] R. Strunz and J. W. Herrmann, "Reliability as an independent variable applied to liquid rocket engine test plans," *J. Propuls. Power*, vol. 27, no. 5, pp. 1032–1044, 2011, doi: 10.2514/1.B34279.

[7] J. S. Hardi *et al.*, "High frequency combustion instabilities in liquid propellant rocket engines : research programme at DLR Lampoldshausen," *Proc. Int. Symp. Thermoacoustic Instab. Ind. meets Acad.*, no. January, pp. 1–11, 2016.

[8] N. T. Standard, "NASA-STD-5012B STRENGTH AND LIFE ASSESSMENT REQUIREMENTS FOR LIQUID-FUELED SPACE PROPULSION SYSTEM ENGINES." 2016.

[9] W. Zhang, *Failure characteristics analysis and fault diagnosis for liquid rocket engines*. 2016. doi: 10.1007/978-3-662-49254-3.

[10] A. Babu, A. . Asraff, and N. Philip, "Fatigue Life Prediction of a Rocket Combustion Chamber," *IOSR J. Mech. Civ. Eng.*, vol. 11, no. 5, pp. 12–20, 2014.

[11] R. B. Hetnarski, *Encyclopedia of Thermal Stresses*. 2014.

[12] A. Babu, A. . Asraff, and N. Philip, "Fatigue Life Prediction of a Rocket Combustion Chamber," *IOSR J. Mech. Civ. Eng.*, vol. 11, no. 5, pp. 12–20, 2014, doi: 10.9790/1684-11521220.

[13] V. Buljak and G. Ranzi, *Constitutive Modeling of Engineering Materials*, 1st Editio.

[14] J. R. Riccius, "Results of a Liquid Rocket Booster (LRB) Nozzle Throat Related Thermo-Mechanical Fatigue (TMF) Panel Test," 2019, pp. 1–6.

[15] J. R. Riccius, G. Thiede, and S. Weitritt, "Liquid booster engine related TMF panel tests," pp. 1–7, 2017, doi: 10.13009/EUCASS2017-659.

[16] P. O. Bouchard, L. Bourgeon, S. Fayolle, and K. Mocellin, "An enhanced Lemaitre model formulation for materials processing damage computation," *Int. J. Mater. Form.*,vol. 4, no. 3, pp. 299–315, 2011, doi:10.1007/s12289-010-0996-5.

[17] N. Bonora, D. Gentile, and A. Pirondi, "Identification of the parameters of a non-linear continuum damage mechanics model for ductile failure in metals," *J. Strain Anal. Eng. Des.*, vol. 39, no. 6, pp. 639–651, 2004, doi: 10.1243/0309324042379356.

[18] N. Bonora, "A NONLINEAR CDM MODEL FOR DUCTILE FAILURE," 1997.

[19] X. Zhang, Z. Chen, and Y. Liu, "Constitutive Models," 2017, pp. 175–219. doi: 10.1016/B978-0-12-407716-4.00006-5.

[20] J. Dufailly and J. Lemaitre, "Modeling Very Low Cycle Fatigue," *International Journal of Damage Mechanics*, vol. 4, no. 2. pp. 153–170, 1995. doi: 10.1177/105678959500400204.

[21] T. Masuoka and J. R. Riccius, "Life evaluation of a combustion chamber by thermomechanical fatigue panel tests based on a creep fatigue and ductile damage model," *Int. J. Damage Mech.*, vol. 29, no. 2, pp. 226–245, 2020.

[22] M. T. Gulczyński, J. R. Riccius, G. Waxenegger-wilfing, J. C. Deeken, and M. Oschwald, "Numerical Fatigue Life Analysis of Combustion Chamber Walls for Future Reusable Liquid Rocket Engines (LREs) Applications," no. SP2022, pp. 1–14, 2022.

[23] U. Sarajärvi and O. Cronvall, *A Procedure to Generate Input Data of Cyclic Softening and Hardening for FEM Analysis from Constant Strain Amplitude Fatigue Tests in LCF Regime*, no. March. 2007.

[24] H. Mahbadi and M. R. Eslami, "Cyclic loading of thick vessels based on the Prager and Armstrong-Frederick kinematic hardening models," *Int. J. Press. Vessel. Pip.*, vol. 83, no. 6, pp. 409–419, 2006, doi: 10.1016/j.ijpvp.2006.02.031.

[25] S. K. Paul, "A critical review of experimental aspects in ratcheting fatigue: microstructure to specimen to component," *J. Mater. Res. Technol.*, vol. 8, no. 5, pp. 4894–4914, 2019, doi: 10.1016/j.jmrt.2019.06.014.

[26] M. T. Gulczyński *et al.*, "Numerical Turbine Blade Fatigue Life Analysis for Reusable Liquid Rocket Engines (LREs) Applications," 2022, no. 9TH EUROPEAN CONFERENCE FOR AERONAUTICS AND SPACE SCIENCES (EUCASS), pp. 1–14. doi: 10.13009/EUCASS2022-6150.

[27] J. R. Riccius, E. B. Zametaev, M. T. Gulczyński, and R. H. S. Hahn, "NUMERICAL LRE TURBINE BLADE FATIGUE LIFE ANALYSIS TAKING INTO ACCOUNT PARTIAL ADMISSION EFFECTS," 2022.

[28] M. T. Gulczyński, J. R. Riccius, G. Waxenegger-Wilfing, J. C. Deeken, and M. Oschwald, "Turbine Blades for Reusable Liquid Rocket Engines (LRE) – Numerical Fatigue Life Investigation," 2023.